Published in final edited form as:
Magn Reson Med. 2009 February ; 61(2): 364–371. doi:10.1002/mrm.21850.

Quantitative Magnetization Transfer Measured Pool Size Ratio Reflects Optic Nerve Myelin Content in *ex vivo* Mice

Xiawei Ou[1,2], **Shu-Wei Sun**[3], **Hsiao-Fang Liang**[3], **Sheng-Kwei Song**[3], and **Daniel F. Gochberg**[1]

[1]Department of Radiology, Vanderbilt University Institute of Imaging Science, Nashville, TN

[2]Arkansas Children's Hospital, University of Arkansas for Medical Sciences, Little Rock, AR

[3]Department of Radiology, Washington University School of Medicine, St. Louis, MO

Abstract

Optic nerves from mice that have undergone retinal ischemia were examined using a newly implemented quantitative magnetization transfer (qMT) technique. Previously published results indicate that the optic nerve from retinal ischemia mice suffered significant axon degeneration without detectable myelin injury at three days after reperfusion. At this time point, we acquired *ex vivo* qMT parameters from both shiverer mice (which have nearly no myelin) and control mice that have undergone retinal ischemia, and these qMT measures were compared with diffusion tensor imaging (DTI) results. Our findings suggests that the qMT estimated ratio of the pool sizes of the macromolecular and free water protons reflected the different myelin contents in the optic nerves between the shiverer and control mice. This pool size ratio was specific to myelin content only and was not significantly affected by the presence of axon injury in mouse optic nerve three days after retinal ischemia.

Keywords

quantitative magnetization transfer; pool size ratio; diffusion tensor imaging; myelin; optic nerve

Introduction

Magnetic resonance imaging (MRI) techniques have been widely used on the diagnosis of white matter diseases in the central nervous system. Conventional T_1, T_2, and proton density weighted imaging provide contrasts to differentiate lesions from normal white matter. More sophisticated imaging techniques, such as magnetization transfer (MT) imaging (1), diffusion tenser imaging (DTI) (2), and multiple components T_2 imaging (3), provide not only contrast but also quantitative information for lesion detection. Though demyelination is the major target of many MRI studies, many white matter diseases are a combination of demyelination and other pathologies, such as edema, gliosis, inflammation, and axon degeneration. It is important to know the specificity of each MRI technique to each of these white matter pathologies.

DTI investigates the microstructures in white matter by characterizing water diffusion anisotropy. Previous results suggest that directional diffusivities from DTI experiments are

Daniel Gochberg Vanderbilt University Institute of Imaging Science 1161 21st Avenue South, Medical Center North, AA-1105 Nashville, TN 37232-2310 Tel: (615) 322-8356 daniel.gochberg@vanderbilt.edu
Xiawei Ou Arkansas Children's Hospital 800 Marshall Street, Slot 105 Little Rock, AR 72202 Tel: (501) 364-4837 ouxiawei@uams.edu

specific to white matter pathology (4-6). The radial diffusivity, which is the apparent water diffusion coefficient in the direction perpendicular to the axonal fibers, may reflect the integrity of the myelin sheaths surrounding the fibers; the axial diffusivity, which is the water apparent diffusion coefficient in the direction parallel to the axonal fibers, may reflect the integrity of the axonal fibers themselves. Shiverer mice brain (which has nearly no myelin in the white matter, but has intact axonal fibers) (7) was imaged by DTI and compared to control mice brain (5,8). Significant differences were found in the radial diffusivity in the white matter, while there was no difference in the axial diffusivity in the white matter. Furthermore, mice optic nerves with retinal ischemia (which has both axonal damage and myelin degeneration during the time course) were examined by DTI (9,10). It was found that at three days after the retinal ischemia, the axial diffusivity of the injured optic nerve was significantly decreased, while the radial diffusivity of the injured optic nerve remained unchanged. The correlated histology results indicated axonal damage but no demyelination. Therefore, mouse optic nerve undergoing retinal ischemia is an excellent animal model to investigate the specificity of MRI techniques on the detection of demyelination while axonal damage is present.

MT is very sensitive to myelin, since it characterizes the interactions between free water protons and macromolecular protons which are associated with myelin lipids (11,12). Magnetization transfer ratio (MTR) is a semi-quantitative parameter which describes the degree of this interaction. MTR equals one minus the ratio of the free water signal with and without an off-resonance rf pulse that selectively saturates the solid-like macromolecular protons. MTR has increased sensitivity to demyelinated lesions over conventional MRI techniques (1). However, MTR values depend on the details of the pulse sequence and they also may be affected by other pathologies, and therefore lack specificity for myelin. Quantitative magnetization transfer (qMT) provides a more direct insight by modeling the underlying properties involved in the MT process (13). All of the relaxation and exchange rates of the free water and macromolecular protons are individually characterized in a qMT model. One of the qMT parameters, the pool size ratio (the ratio of the number of bound macromolecular protons to the free water protons), is independent of pulse sequence details and may be a more direct measure of myelin. For example, the pool size ratio measurement reflects the dysmyelination of shiverer mice brain (8) and spinal cord (14).

Determining the specificity of MT parameters to the underlying biophysical conditions is complicated by the typical coupling of pathological features. For example, though demyelination is the dominating pathology that affects the qMT parameters, the role of other pathologies such as inflammation on qMT measurements needs to be considered. Stanisz et al (15) examined the qMT properties in inflamed neural tissues, and found that the pool size ratio is not the best indicator of demyelination when inflammation is also present, not only due to the increase in the number of extra-myelin water protons by inflammation, but also due to the change in the MT properties caused by the pH change in the inflamed sample. Odrobina et al (16) measured the qMT parameters for ex vivo demyelinated rat sciatic nerve and confirmed the correlation between myelin fraction and the pool size ratio, but also noted the difficulty of separating demyelination from inflammation by qMT alone. Tozer et al (17) also correlated the pool size ratio in the qMT measurements with the myelin water fraction in the multiple component T2 measurements for human subjects. They suggested that it is still valuable to perform both measurements to increase the specificity of those parameters to demyelination with existing inflammation.

Changes in axon integrity may also influence qMT measurements of demyelination. However, most current studies are limited to the relation of axonal damage to MTR, not to qMT parameters. For example, Schmierer et al measured the MTR in postmortem multiple sclerosis brain with the addition of quantitative pathological studies (18). They found

significant correlation not only between myelin content and MTR, but also between myelin content and axonal count. However, it was not clear how axon count changes and myelin content changes separately affect the semi-quantitative MTR measurement, nor did they address how the axon count changes affect the quantitative MT measurements. Post mortem studies of the spinal cord of multiple sclerosis patients by Mottershead et al also revealed strong correlations of reduced myelin content and axonal loss to reduced MTR (19), but again without separating the effects of demyelination and axonal loss. In contrast, Blerzer et al investigated the quantitative MRI and pathology correlations of brain white matter lesions in experimental autoimmune encephalomyelitis (EAE) non-human primates, and their results showed that the correlation of axonal density with MTR was insignificant (20). Hickman et al (21) performed MT imaging in acute optic neuritis patients and found that MTR values did not change at the onset, when visual impairment was at its worst. They proposed that this lack of change was possibly due to the acute axonal degeneration transiently increasing MTR and other pathologies decreasing MTR. Their suggested possibility of conflicting pathologies shows the need for animal studies with separated and controlled pathologies. In summary, both appropriately specific animal models and more specific MR measures (i.e. the qMT measured pool size ratio) may be necessary to evaluate the correlations between demyelination measurements and changes of axonal pathology.

In this paper, we utilized *ex vivo* samples with known axonal damage without demyelination, mice optic nerve at three days after retinal ischemia (9,10), to test the dependency of the pool size ratio measured by qMT on axonal degeneration alone. We acquired data on both shiverer and control mice, and both normal and injured optic nerves to investigate both the sensitivity and specificity of the pool size ratio on demyelination as separated from axonal degeneration. DTI and histology studies were also performed to provide a separate measure of the pathology.

Theory

We chose the recently developed SIR-FSE method (22) to perform the qMT measurements. This technique uses a fast spin echo pulse sequence with a preceding 180 degree inversion pulse. Unlike the widely used pulsed saturation method (23), which manipulates the restricted macromolecular spins, SIR-FSE selectively inverts the free liquid spins. As a result of MT, the free recovery of the liquid spins after the inversion pulse is bi-exponential (with fast and slow recovery rates on the order of magnitude of 25 Hz and 1 Hz, respectively) instead of single exponential (24). A series of inversion times are used to model the transient signal of the bi-exponential recovery after the inversion pulse. A constant pre-delay time t_d (the time delay after the fast spin echo acquisition in each repetition), instead of a constant repetition time *TR*, allows a determination of the qMT parameters when starting from non-equilibrium conditions and resulting in greater SNR efficiency (22).

For a two-pool system (immobile macromolecular protons and free water protons) such as brain tissue, the recovery of the inverted free pool magnetization after the inversion pulse is (22):

$$\frac{M_f(t)}{M_{f\infty}} = b_f^+ \exp\left(-R_1^+ t\right) + b_f^- \exp\left(-R_1^- t\right) + 1 \quad [1]$$

where

$$2R_1^{\pm}=R_{1f}+R_{1m}+k_{fm}+k_{mf} \pm \sqrt{\left(R_{1f}-R_{1m}+k_{fm}-k_{mf}\right)^2+4k_{fm}k_{mf}} \quad [2]$$

R_1^- and R_1^+ are the slow and fast recovery rates, respectively. The subscripts f and m refer to the free and macromolecular proton pools, respectively. $M_f(t)$ and $M_m(t)$ are the longitudinal magnetizations with equilibrium values $M_{f\infty}$ and $M_{m\infty}$. R_{1f} and R_{1m} are the longitudinal relaxation rates of the free and macromolecular protons when there is no magnetization transfer between them. k_{fm} is the magnetization exchange rate from the free pool to the macromolecular pool, k_{mf} is the rate from the macromolecular pool to the free pool, and k_{fm}/k_{mf} is equal to the pool size ratio (p_m/p_f).

k_{mf} is usually much larger than any other rate, and a Taylor expansion gives the approximations(25):

$$k_{mf} \approx R_1^+ \text{and} \quad \frac{P_m}{P_f} \approx \frac{b_f^+}{\left(b_f^+ + b_f^- + 1 - S_m\left(1-e^{-R_1^- t_d}\right)\right)} \quad [3]$$

In the experiments $R_1^+, R_1^-, b_f^+, \text{and} b_f^-$ are determined by fitting the measured images to Eq [1], where t is the varied inversion time. The qMT parameters are then calculated from Eq [3], where t_d is the constant predelay, S_m is the simulated saturation effect of the rf pulse (0.41 ± 0.11 for a 1 ms sinc inversion pulse on a solid pool with a Gaussian lineshape and a T_2 between 10 μs and 20 μs, calculated by the same method as described in (26,27)). Being an on-resonance method, the results have little dependence on the assumed lineshape, as discussed in previous publications (22).

The Diffusion tensor (**D**) can be derived according to Eq [4], where S is the diffusion-weighted signal, S_0 is signal with diffusion weighting factor b = 0 , and **n** represents the encoding directions (28). The resulting tensor element maps can be used to derive eigenvalues ($\lambda_1,\lambda_2,\lambda_3$) of the diffusion tensor by matrix diagonalization. Quantitative indices including axial diffusivity (λ_P), radial diffusivity ($\lambda_\perp$), and relative anisotropy (RA), can be derived according to following equations:

$$S=S_0 \quad \exp\left(-b \cdot \mathbf{n} \cdot \mathbf{D} \cdot \mathbf{n}^T\right) \quad [4]$$

$$\lambda=\lambda_1 \quad [5]$$

$$\lambda_\perp=0.5 \times (\lambda_2+\lambda_3) \quad [6]$$

$$RA=\frac{\sqrt{(\lambda_1 - Tr(\mathbf{D})/3)^2+(\lambda_2 - Tr(\mathbf{D})/3)^2+(\lambda_3 - Tr(\mathbf{D})/3)^2}}{Tr(\mathbf{D})/\sqrt{3}} \quad [7]$$

Methods

Animal preparation

All procedures were in compliance with the National Institute of Health Guide for the Care and Use of Laboratory Animals, as well as institutional policies and guidelines. Unilateral retinal ischemia was induced in five shiverer and six control mice. Briefly, 100 – 120 mmHg intraocular pressure was applied to the left eye of each mouse for one hour by inserting into the anterior chamber a 32-gauge needle connected to a saline reservoir placed above the eye. Reperfusion started immediately after removal of the cannula. At three days after the retina ischemia, all mice were euthanized and perfused through the left cardiac ventricle with phosphate-buffered saline (PBS) followed by 10% formalin/PBS solution. The mice were decapitated and their heads were kept in 10% formalin/PBS solution and stored at 4°C for one week. Just before imaging, each mouse head was transferred to a 10 mm diameter cylinder filled with PBS solution.

Data Acquisition

Cylinders with fixed mouse head were placed in a 1 cm inner diameter solenoid coil which serves as both RF transmitter and receiver, and data from one coronal slice which contains both optic nerves were acquired in a 4.7 T Varian UNITY INOVA spectrometer with an actively shielded Magnex gradient coil (10 cm inner diameter, 60 G/cm, 100 μs rise time). A fast spin echo sequence with a 1 ms sinc inversion pulse was used for the qMT experiments. 18 images with the inversion times ranging from 5 ms to 7.9 s were obtained with 2 s constant pre-delay, 8 averages, 16 echoes (with zero phase encode in the first echo), 10 ms echo spacing time, 25 mm by 25 mm field of view, 0.8 mm thick slice, and 256×256 data matrix zero-filled to 512×512. The imaging slice was chosen at a position which was about 1 – 1.5 mm anterior from the optic chiasm. This position was also chosen for the histology study to ensure the MRI slice matches the histology slice. The total imaging time was 2 hours. Data were fitted to the bi-exponential function of the inversion times (Eq [1]) to determine qMT parameters pixel by pixel. The goodness of qMT data fitting was ensured by setting a criteria to the fitting residue versus signal, specifically, $\sqrt{\frac{1}{18}\sum \text{residue}^2}/\text{signal}\,(t_i{=}7.9s) \le 0.01$. Almost all pixels met this criteria except a few boundary pixels which were excluded in the data analysis.

A diffusion weighted spin echo pulse sequence with 1 s repetition time, 4 averages, 38 ms echo time, 13 ms time between gradient pulses, 4 ms diffusion gradient duration, b value of 1.879 $ms / \mu m^2$, diffusion sensitizing gradients along six directions (x,y,z) = (1,1,0), (0,1,1), (1,0,1), (-1,1,0), (0,-1,1), (1,0,-1), plus an image with no diffusion gradients, and the same spatial resolution as in the qMT experiments was used to acquire data (the scan time was 2 hours). On a pixel-by-pixel basis, the axial diffusivity (λ), radial diffusivity ($\lambda_\perp$), and relative anisotropy (RA), as defined by Eqs [5]-[7], were derived using software written in Matlab (MathWorks, Natick, MA, USA).

Statistical Analysis

For each qMT and DTI parameter, statistically significant difference between the injured and uninjured optic nerves was evaluated by a two-tailed student t-test. The t value was calculated by the means and standard deviations of each parameter in control/shiverer mice optic nerves. With the t-value and the known degree of freedom (6 control mice and 5 shiver mice gave a degree of freedom equals 9), the probability (p-value) that each parameter being the same between the control and the injured optic nerves was determined.

Histology Study

After MRI studies, 4 mm thick coronal tissue blocks were obtained from each control and shiverer mouse brain and embedded in paraffin. 3 μm thick slices matching the MRI slices were cut and deparaffinized in xylene for immunohistochemical examinations. The integrity of myelin was assessed by using a primary antibody against myelin basics protein (MBP, 1:250; Zymed Laboratories Inc., South San Francisco, CA). The integrity of axon was assessed by using a primary antibody against phosphorylated neurofilament (pNF, SMI-31, 1:1000; Sternberger Monoclonals, Lutherville, MD). Following 15 minutes wash in PBS, slices were incubated in fluorescent secondary antibodies for one hour at room temperature (1:200, anti-rabbit conjugated to Texas Red for MBP, 1:200, anti-mouse conjugated to Alexa 488 for SMI-31; Molecular Probes). Histological sections were examined with a Nikon Eclipse 80i microscope equipped with a 60x oil objective, and digital images were captured with a Photometrics CCD digital camera using MetaMorph image acquisition software (Universal Imaging Corporation, Downington, PA). The MBP and SMI-31 positive axons were counted in a blinded fashion. Images captured from the center of each optic nerve were displayed using MetaMorph. Both the red MBP positive staining ring representing the myelinated axon and the green SMI-31 positive staining dot representing the normal axon were counted. The axon counting was conducted through the entire captured image (110μm×110μm).

Results

Figure 1 shows a T_2 weighted image, a relative anisotropy map from the DTI experiments, and a pool size ratio map from the qMT experiments for a control mouse. The resulting qMT and DTI parameters for all mice are listed in Table 1.

qMT and DTI results

The pool size ratios in the control mice optic nerves are much higher than those in the shiverer mice optic nerves (30% difference for the injured optic nerves, p = 0.0001; 24% difference for the uninjured optic nerves, p = 0.008). There is nearly no pool size ratio difference (3%, p = 0.70) between the left (injured) and right (uninjured) optic nerves in the control mice, while there is insignificant difference (10%, p = 0.07) in the shiverer mice. The slow rates (the reciprocal of T_1, which is the longitudinal relaxation time of the sample as one would measure using inversion recovery methods with relatively long t_i values) and fast rates (approximately equals the MT exchange rate from macromolecular protons to free water protons) in all mice are similar between the injured and uninjured optic nerves.

The radial diffusivities are the same between the injured and uninjured optic nerves (no difference, p = 0.90 for the control mice; no difference, p = 0.84 for the shiverer mice). Meanwhile, the radial diffusivities in the shiverer mice are much higher than those in the control mice (23% difference for the injured optic nerves, p = 0.03; 23% difference for the uninjured optic nerves, p = 0.06). For the axial diffusivities, there are significant differences (33% for the control mice, p = 0.006; 26% for the shiverer mice, p = 0.0002) between the injured optic nerves and the uninjured optic nerves. Meanwhile, the axial diffusivities in the shiverer mice optic nerves are slightly and insignificantly higher than those in the control mice optic nerves (9% difference for the injured nerves, p = 0.35; 8% difference for the uninjured nerves, p = 0.17). For the relative anisotropy, there are significant differences (27% for the control mice, p = 0.0011; 27% for the shiverer mice, p = 0.0005) between the injured and uninjured optic nerves, while there are small differences (8% for the injured nerves, p = 0.16; 6% for the uninjured nerves, p = 0.17) between the control and shiverer mice.

Histological Study Results

Immunohistochemistry exhibited that reduction of the positive staining to pNF in injured optic nerves suggestive of the axonal damage at 3 days after retinal ischemia (Fig 2). Despite the absence of myelin (stained by MBP) in shiverer mice, both control and shiverer mice showed similar degree of axonal damage in the injured optic nerves, where 82 ± 12% ($p < 0.05$) and 75 ± 12% ($p < 0.05$) reductions of the pNF counts were measured from control and shiverer mice, respectively (Fig 3). For the control mice, the MBP staining result in the injured optic nerves is similar to that in the uninjured optic nerves, suggesting that there was no demyelination in the injured optic nerves.

Discussion

It has been shown that white matter abnormalities may cause increased T_1 and T_2, decreased MTR, and changes of diffusion properties including RA, FA, and ADC (2,29,30). Those parameters are sensitive to both myelin and axon pathologies, and they are not able to differentiate the effects of demyelination and axonal degeneration. Though both pathologies usually accompany each other, they might develop at different stages and have different consequences. For example, it has been suggested that demyelination is the dominating pathology for the relapsing-remitting multiple sclerosis, while axonal degeneration is the dominating factor for the irreversible chronic-progressive multiple sclerosis (31). Therefore, MRI techniques that distinguish demyelination with axonal degeneration are essential for diagnosis and clinic applications.

Radial diffusivity and axonal diffusivity may reflect the integrity of the myelin sheath and axon tracts, respectively (4-6,9,10,32). Meanwhile, the pool size ratio in qMT measurements is suggested to be highly related to myelin contents (8), and it is also a possible marker to differentiate the pathological changes in myelin sheath/axon tracts. qMT and DTI studies have been performed on control/shiverer mice corpus callosum. Both the pool size ratio and the radial diffusivity are sensitive to the myelin sheath of axonal fibers, and these two parameters correlate to each other (8). In this study, our findings on mice optic nerves support theses previous results. The percentage difference in macromolecular proton pool size ratios between control and shiverer is smaller than that measured in shiverer mice spinal cord by pulsed MT measurements (14), which may reflect differences between brain and spinal cord, sample preparation, or qMT acquisition method. The pool size ratios in the control mice optic nerves (both the injured and uninjured nerves) are significantly higher than those in the shiverer mice optic nerves, correlating with the lack of myelin in the shiverer mice optic nerves. On the other hand, the radial diffusivities in the control mice optic nerves (both the injured and uninjured nerves) are significantly lower than those in the shiverer mice optic nerves, also indicating the lack of myelin in the shiverer mice optic nerves. Furthermore, the changes of pool size ratio and radial diffusivity are of a similar percentage, which is consistent with our previous results on mice corpus callosum. Our results confirm that both the pool size ratio and radial diffusivity correlate with the integrity of myelin in mice optic nerves.

For qMT parameters other than the pool size ratio, the slow rates (which are equivalent to the measured R_1 of studies that employ only large t_i values) in the optic nerves are lower than the slow rates in the corpus callosum we measured previously (8). However, the slow rates in the control mice optic nerves are slightly higher than those in the shiverer mice optic nerves, consistent with previous corpus callosum results. The slow rate difference between the control and shiverer mice optic nerves is small, indicating that T_1 is not an optimal marker for myelin. Nor is the fast recovery rate (which by Eq [3] is roughly equal to k_{mf}, and sometimes referred to as R (13)), since it is not differentiated between the control and shiverer mice optic nerves. For DTI parameters, the diffusivities measured in our

experiments are significantly lower than those from *in vivo* mice optic nerve (9) and *ex vivo* bovine optic nerve measured within 2 hours post mortem without fixation (33). This low diffusivity is probably due to the formalin fixation effects (34). Nevertheless, the diffusion anisotropy is likely preserved after fixation (32,34). We did not see any obvious change of axial diffusivities in the corpus callosum between the control and shiverer mice previously, but we did see small changes (8-9%) of axial diffusivities in the optic nerves between the control and shiverer mice. This may be due to the partial volume effects and the limited size of the ROI. In any case, the p values for the axial diffusivity in the optic nerves range from 0.17 to 0.35, indicating no significant difference. These values are also comparable to the p value ($p = 0.27$) previously calculated from the corpus callosum axial diffusivities between the control and shiverer mice (8). The relative anisotropies in control mice optic nerves are higher than those in shiverer mice optic nerves, which is consistent with previous mice brain results, though more significant difference was observed in mice corpus callosum. In general, the qMT and DTI analysis on the dysmyelinated shiverer and the myelinated control mice optic nerves agrees well with our previous analysis on the shiverer/control mice corpus callosums.

Optic nerve contains dense packed myelin sheath around the axonal fibers and has no crossing fiber tracts. After the retinal ischemia surgery, the degenerations of myelin and axon fiber start at different time points and proceed at different rates. In general, at three days after the ischemia, axonal degeneration is significant, but demyelination is absent (9,10). The separation of these two pathologies provides an excellent model to evaluate the specificity of qMT and DTI parameters to myelin. From our DTI results, the radial diffusivity (which previous results (5,6,8,9) indicate may be sensitive to myelin) is the same in the injured optic nerves and the uninjured optic nerves, and for both control and shiverer mice. These similar radial diffusivities indicate the lack of demyelination, which is confirmed by the MBP immunostaining results. On the other hand, the axial diffusivity, which may reflect the axonal fiber integrity (4,9,10), is significantly different between the injured and uninjured optic nerves, indicating that noticeable axonal degeneration is present in the injured optic nerves, which is in agreement with the Neurofilament labeling results. There is also significant difference for the relative anisotropy between the injured and uninjured optic nerves, due to the difference of the axial diffusivity since the radial diffusivity is unchanged.

With the confirmation of Histology and DTI results that there is axonal degeneration but no demyelination, qMT measurements were performed on this animal model to check if there is any effect on the qMT parameters caused by the presence of axonal degeneration. We did not see any significant difference in the measured pool size ratios between the injured and the uninjured optic nerves for the control mice, which suggests that axonal degeneration did not play a role in the detection of demyelination in the control mice by qMT measurements. For the shiverer mice, the uninjured optic nerves have slightly higher pool size ratio than the injured optic nerves. Since shiverer mice have nearly no myelin in their optic nerves, the source of this difference is from the contribution to the pool size ratio by pathologies other than demyelination. While our results indicate that changes in the pool size ratio principally reflect myelin changes, some dependence on non-myelin bio-structures is likely. For example, the pool size ratio of gray matter is not zero, and it is also not zero for the dysmyelinated shiverer mice white matter (8). However, any pool size ratio dependence on changes in non-myelin bio-structures in this model is small (9% difference between the injured and uninjured optic nerves of the shiverer mice) and of relatively low significance ($p = 0.07$). Furthermore, our results also show that the slow and fast rates remain the same for the injured optic nerves when comparing to the uninjured optic nerves. Therefore, in general, the qMT measurements were not significantly affected by the lone presence of axonal degeneration in our experiment.

qMT maps of healthy subjects were produced by different groups. Sled et al show that the pool size ratio in white and gray matter regions are significantly different (35); Yarnykh et al were able to show the appearance of the major fiber tracts on the pool size ratio map, and therefore to show that pool size ratio is associated with the density of fiber tracts (36). Yarnykh's results are not contradictory to ours, as the myelin sheath density also increases with increases in the fiber tract density. We were not able to see fiber tracts in the white matter of our pool size ratio maps due to the small size of mice brain and the relatively large voxel size for microstructures imaging, but we were able to show that the pool size ratio measurement generally will not be affected by the axonal damage in the injured optic nerves. We believe that the density change of axonal fibers will affect qMT measurements because of the consequent myelin sheath density change, but the axonal degeneration caused by fiber transection will not affect qMT measurements.

Narayanan et al measured the pool size ratio in normal appearing white matter (NAWM) of MS patients via the pulse saturation technique (37). In addition to myelin detection by qMT, they also measured the resonance intensities of N-acetylaspartate (NAA) relative to creatine (Cr) to investigate the axonal injury. They found no correlation between the pool size ratio (putative myelin marker) and the NAA/Cr ratio (putative axonal intensity marker). Their results are consistent with axonal injury in the NAWM (i.e. the Wallerian degeneration of transected axons) not paralleling demyelination. The variation of the measured pool size ratio in the NAWM was small in their experiments, also implying that the existing axonal degeneration does not affect the pool size ratio measurement.

While our results are consistent with these human *in vivo* measurements, a full knowledge of the specificity of diffusion tensor and qMT imaging methods will require a range of animal studies where the relative degrees of demyelination, axonal loss, gliosis, and edema are varied. This study fills in a data point by comparing qMT and diffusion tensor results in an animal model separating the effects of demyelination and axonal degeneration. However, inflammation effects cannot be separated from demyelination effects by this method. In general, the pathological specificity of a particular method in a particular animal model will depend on the concurrent biophysical changes, and modeling such changes may provide insight into expected correlations. While neurofilaments and axoplasm have a small effect on water diffusion, the primary determinant of diffusion tensor imaging in white matter is the restrictive effects of membranes (38). DTI will reflect pathologies only to the degree to which they affect water transport. While there have been a few studies modeling diffusion of myelin associated water (39-41), this water component, with its short T_2, likely plays only a small direct role in diffusion measurements of white matter, and instead myelin plays the role of a diffusion barrier. A third leading method for myelin specific imaging not included in this study is multi-exponential T_2(MET) and, like qMT, it is affected by the strong water-macromolecular coupling via the cholesterol in the lipid bilayers of myelin in white matter (42), and, therefore, these two methods may be expected to show similar sensitivity and specificity to various pathologies. Four pool modeling studies of white matter (43,44), however, have given inconsistent results on whether there is an underlying biophysical basis for qMT-MET correlation.

Conclusion

We implemented selective inversion recovery fast spin echo (SIR-FSE) quantitative magnetization transfer (qMT) imaging technique to investigate the integrity of myelin in optic nerves after retinal ischemia in control and shiverer mice. We found that at three days after the ischemia there was significant axonal degeneration in mice optic nerves, but no detectable demyelination. Our qMT measurements sensitivity to myelin was not significantly affected by the axonal injury, as indicated by the control versus shiverer qMT

results. In addition, qMT parameters were similar between the injured optic nerves and uninjured optic nerves. Our results suggest that the key qMT parameter, the pool size ratio, is not only sensitive but also specific to demyelination even when axonal injury is co-existing.

Acknowledgments

NIH R01EB001452, R01NS047592, R01NS054194, NMSS RG 3864, NMSS CA 1012.

Reference

1. Dousset V, Grossman RI, Ramer KN, Schnall MD, Young LH, Gonzalezscarano F, Lavi E, Cohen JA. Experimental allergic encephalomyelitis and multiple sclerosis - lesion characterization with magnetization transfer imaging. Radiology. 1992; 182(2):483–491. [PubMed: 1732968]
2. Filippi M, Cercignani M, Inglese M, Horsfield MA, Comi G. Diffusion tensor magnetic resonance imaging in multiple sclerosis. Neurology. 2001; 56(3):304–311. [PubMed: 11171893]
3. Mackay A, Whittall K, Adler J, Li D, Paty D, Graeb D. In-vivo visualization of myelin water in brain by magnetic resonance. Magnetic Resonance in Medicine. 1994; 31(6):673–677. [PubMed: 8057820]
4. Kim JH, Budde MD, Liang HF, Klein RS, Russell JH, Cross AH, Song SK. Detecting axon damage in spinal cord from a mouse model of multiple sclerosis. Neurobiol Dis. 2006; 21(3):626–632. [PubMed: 16298135]
5. Song SK, Sun SW, Ramsbottom MJ, Chang C, Russell J, Cross AH. Dysmyelination revealed through MRI as increased radial (but unchanged axial) diffusion of water. Neuroimage. 2002; 17(3): 1429–1436. [PubMed: 12414282]
6. Song SK, Yoshino J, Le TQ, Lin SJ, Sun SW, Cross AH, Armstrong RC. Demyelination increases radial diffusivity in corpus callosum of mouse brain. Neuroimage. 2005; 26(1):132–140. [PubMed: 15862213]
7. Privat A, Jacque C, Bourre JM, Dupouey P, Baumann N. Absence of the major dense line in myelin of the mutant mouse shiverer. Neuroscience Letters. 1979; 12(1):107–112. [PubMed: 460693]
8. Ou X, Sun SW, Liang HF, Gochberg DF, Song SK. QMT estimated pool size ratio and DTI derived radial diffusivity reflect the integrity of myelin sheath in mice. Pro. Intl. Soc. Magn. Reson. Med. 2007:317.
9. Song SK, Sun SW, Ju WK, Lin SJ, Cross AH, Neufeld AH. Diffusion tensor imaging detects and differentiates axon and myelin degeneration in mouse optic nerve after retinal ischemia. Neuroimage. 2003; 20(3):1714–1722. [PubMed: 14642481]
10. Sun SW, Liang HF, Le TQ, Armstrong RC, Cross AH, Song SK. Differential sensitivity of in vivo and ex vivo diffusion tensor imaging to evolving optic nerve injury in mice with retinal ischemia. Neuroimage. 2006; 32(3):1195–1204. [PubMed: 16797189]
11. Wolff SD, Balaban RS. Magnetization transfer contrast (MTC) and tissue water proton relaxation in vivo. Magn Reson Med. 1989; 10(1):135–144. [PubMed: 2547135]
12. Koenig SH, Brown RD 3rd, Spiller M, Lundbom N. Relaxometry of brain: why white matter appears bright in MRI. Magn Reson Med. 1990; 14(3):482–495. [PubMed: 2355830]
13. Henkelman RM, Huang XM, Xiang QS, Stanisz GJ, Swanson SD, Bronskill MJ. Quantitative interpretation of magnetization transfer. Magnetic Resonance in Medicine. 1993; 29(6):759–766. [PubMed: 8350718]
14. Portnoy S, Stanisz GJ. Modeling pulsed magnetization transfer. Magn Reson Med. 2007; 58(1): 144–155. [PubMed: 17659607]
15. Stanisz GJ, Webb S, Munro CA, Pun T, Midha R. MR properties of excised neural tissue following experimentally induced inflammation. Magnetic Resonance in Medicine. 2004; 51(3):473–479. [PubMed: 15004787]
16. Odrobina EE, Lam TY, Pun T, Midha R, Stanisz GJ. MR properties of excised neural tissue following experimentally induced demyelination. NMR Biomed. 2005; 18(5):277–284. [PubMed: 15948233]

17. Tozer DJ, Davies GR, Altmann DR, Miller DH, Tofts PS. Correlation of apparent myelin measures obtained in multiple sclerosis patients and controls from magnetization transfer and multicompartmental T-2 analysis. Magnetic Resonance in Medicine. 2005; 53(6):1415–1422. [PubMed: 15906291]

18. Schmierer K, Scaravilli F, Altmann DR, Barker GJ, Miller DH. Magnetization transfer ratio and myelin in postmortem multiple sclerosis brain. Ann Neurol. 2004; 56(3):407–415. [PubMed: 15349868]

19. Mottershead JP, Schmierer K, Clemence M, Thornton JS, Scaravilli F, Barker GJ, Tofts PS, Newcombe J, Cuzner ML, Ordidge RJ, McDonald WI, Miller DH. High field MRI correlates of myelin content and axonal density in multiple sclerosis--a post-mortem study of the spinal cord. J Neurol. 2003; 250(11):1293–1301. [PubMed: 14648144]

20. Blezer EL, Bauer J, Brok HP, Nicolay K, t Hart BA. Quantitative MRI-pathology correlations of brain white matter lesions developing in a non-human primate model of multiple sclerosis. NMR Biomed. 2007; 20(2):90–103. [PubMed: 16948176]

21. Hickman SJ, Toosy AT, Jones SJ, Altmann DR, Miszkiel KA, MacManus DG, Barker GJ, Plant GT, Thompson AJ, Miller DH. Serial magnetization transfer imaging in acute optic neuritis. Brain. 2004; 127(Pt 3):692–700. [PubMed: 14736754]

22. Gochberg DF, Gore JC. Quantitative magnetization transfer imaging via selective inversion recovery with short repetition times. Magn Reson Med. 2007; 57(2):437–441. [PubMed: 17260381]

23. Sled JG, Pike GB. Quantitative interpretation of magnetization transfer in spoiled gradient echo MRI sequences. Journal of Magnetic Resonance. 2000; 145(1):24–36. [PubMed: 10873494]

24. Edzes HT, Samulski ET. Measurement of cross-relaxation effects in proton NMR spin-lattice relaxation of water in biological systems - hydrated collagen and muscle. Journal of Magnetic Resonance. 1978; 31(2):207–229.

25. Gochberg DF, Gore JC. Quantitative imaging of magnetization transfer using an inversion recovery sequence. Magn Reson Med. 2003; 49(3):501–505. [PubMed: 12594753]

26. Gochberg DF, Kennan RP, Gore JC. Quantitative studies of magnetization transfer by selective excitation and T-1 recovery. Magnetic Resonance in Medicine. 1997; 38(2):224–231. [PubMed: 9256101]

27. Gochberg DF, Kennan RP, Robson MD, Gore JC. Quantitative imaging of magnetization transfer using multiple selective pulses. Magn Reson Med. 1999; 41(5):1065–1072. [PubMed: 10332891]

28. Basser PJ, Pierpaoli C. Microstructural and physiological features of tissues elucidated by quantitative-diffusion-tensor MRI. J Magn Reson B. 1996; 111(3):209–219. [PubMed: 8661285]

29. Horsfield MA, Jones DK. Applications of diffusion-weighted and diffusion tensor MRI to white matter diseases - a review. Nmr in Biomedicine. 2002; 15(7-8):570–577. [PubMed: 12489103]

30. Miller DH, Grossman RI, Reingold SC, McFarland HF. The role of magnetic resonance techniques in understanding and managing multiple sclerosis. Brain. 1998; 121:3–24. [PubMed: 9549485]

31. Trapp BD, Bo L, Mork S, Chang A. Pathogenesis of tissue injury in MS lesions. J Neuroimmunol. 1999; 98(1):49–56. [PubMed: 10426362]

32. Sun SW, Neil JJ, Song SK. Relative indices of water diffusion anisotropy are equivalent in live and formalin-fixed mouse brains. Magnetic Resonance in Medicine. 2003; 50(4):743–748. [PubMed: 14523960]

33. Henkelman RM, Stanisz GJ, Kim JK, Bronskill MJ. Anisotropy of NMR properties of tissues. Magn Reson Med. 1994; 32(5):592–601. [PubMed: 7808260]

34. Sun SW, Neil JJ, Liang HF, He YY, Schmidt RE, Hsu CY, Song SK. Formalin fixation alters water diffusion coefficient magnitude but not anisotropy in infarcted brain. Magn Reson Med. 2005; 53(6):1447–1451. [PubMed: 15906292]

35. Sled JG, Levesque I, Santos AC, Francis SJ, Narayanan S, Brass SD, Arnold DL, Pike GB. Regional variations in normal brain shown by quantitative magnetization transfer imaging. Magn Reson Med. 2004; 51(2):299–303. [PubMed: 14755655]

36. Yarnykh VL, Yuan C. Cross-relaxation imaging reveals detailed anatomy of white matter fiber tracts in the human brain. Neuroimage. 2004; 23(1):409–424. [PubMed: 15325389]

37. Narayanan S, Francis SJ, Sled JG, Santos AC, Antel S, Levesque I, Brass S, Lapierre Y, Sappey-Marinier D, Pike GB, Arnold DL. Axonal injury in the cerebral normal-appearing white matter of patients with multiple sclerosis is related to concurrent demyelination in lesions but not to concurrent demyelination in normal-appearing white matter. Neuroimage. 2006; 29(2):637–642. [PubMed: 16126413]

38. Beaulieu C, Allen PS. Water diffusion in the giant axon of the squid: implications for diffusion-weighted MRI of the nervous system. Magn Reson Med. 1994; 32(5):579–583. [PubMed: 7808259]

39. Stanisz GJ, Henkelman RM. Diffusional anisotropy of T2 components in bovine optic nerve. Magn Reson Med. 1998; 40(3):405–410. [PubMed: 9727943]

40. Peled S, Cory DG, Raymond SA, Kirschner DA, Jolesz FA. Water diffusion, T(2), and compartmentation in frog sciatic nerve. Magn Reson Med. 1999; 42(5):911–918. [PubMed: 10542350]

41. Andrews TJ, Osborne MT, Does MD. Diffusion of myelin water. Magn Reson Med. 2006; 56(2): 381–385. [PubMed: 16767712]

42. Koenig SH. Cholesterol of myelin is the determinant of gray-white contrast in MRI of brain. Magn Reson Med. 1991; 20(2):285–291. [PubMed: 1775053]

43. Stanisz GJ, Kecojevic A, Bronskill MJ, Henkelman RM. Characterizing white matter with magnetization transfer and T-2. Magnetic Resonance in Medicine. 1999; 42(6):1128–1136. [PubMed: 10571935]

44. Bjarnason TA, Vavasour IM, Chia CL, MacKay AL. Characterization of the NMR behavior of white matter in bovine brain. Magn Reson Med. 2005; 54(5):1072–1081. [PubMed: 16200557]

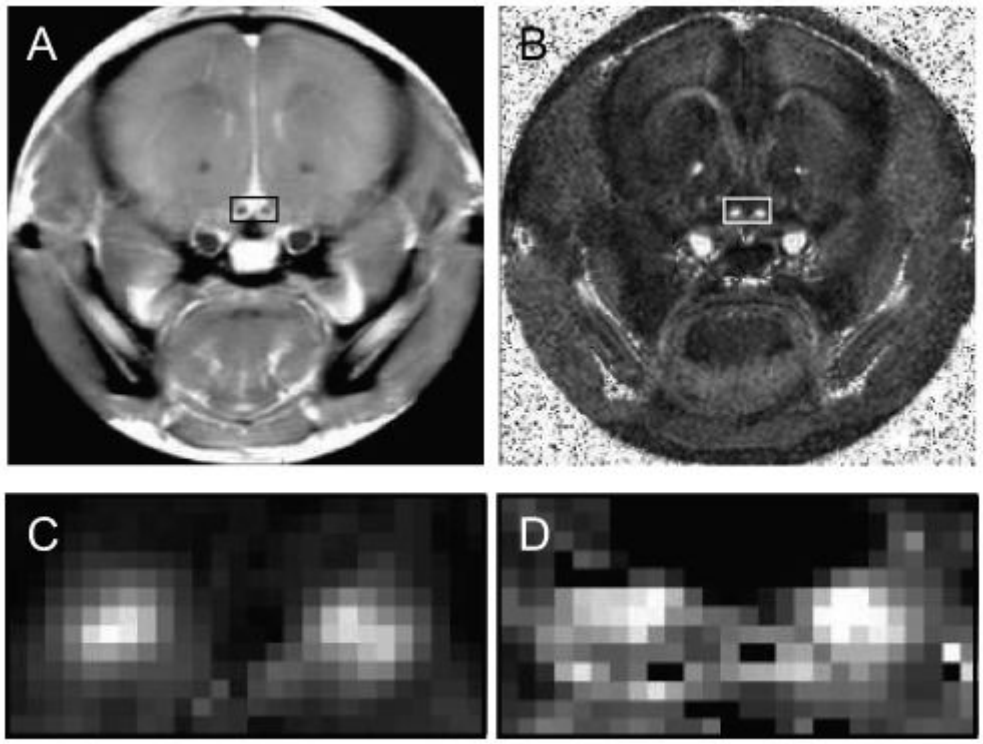

Figure 1.
A): the T_2 weighted image of one coronal slice from a control mouse. Optic nerves are located inside the small rectangle. B): the relative anisotropy map of the same slice from this mouse. C): magnified relative anisotropy map inside the small rectangle. D): magnified pool size ratio map. RA maps have the best contrast between the optic nerve and surrounding tissues, therefore they were used to determine the position of the optic nerves and choose ROIs for each mouse.

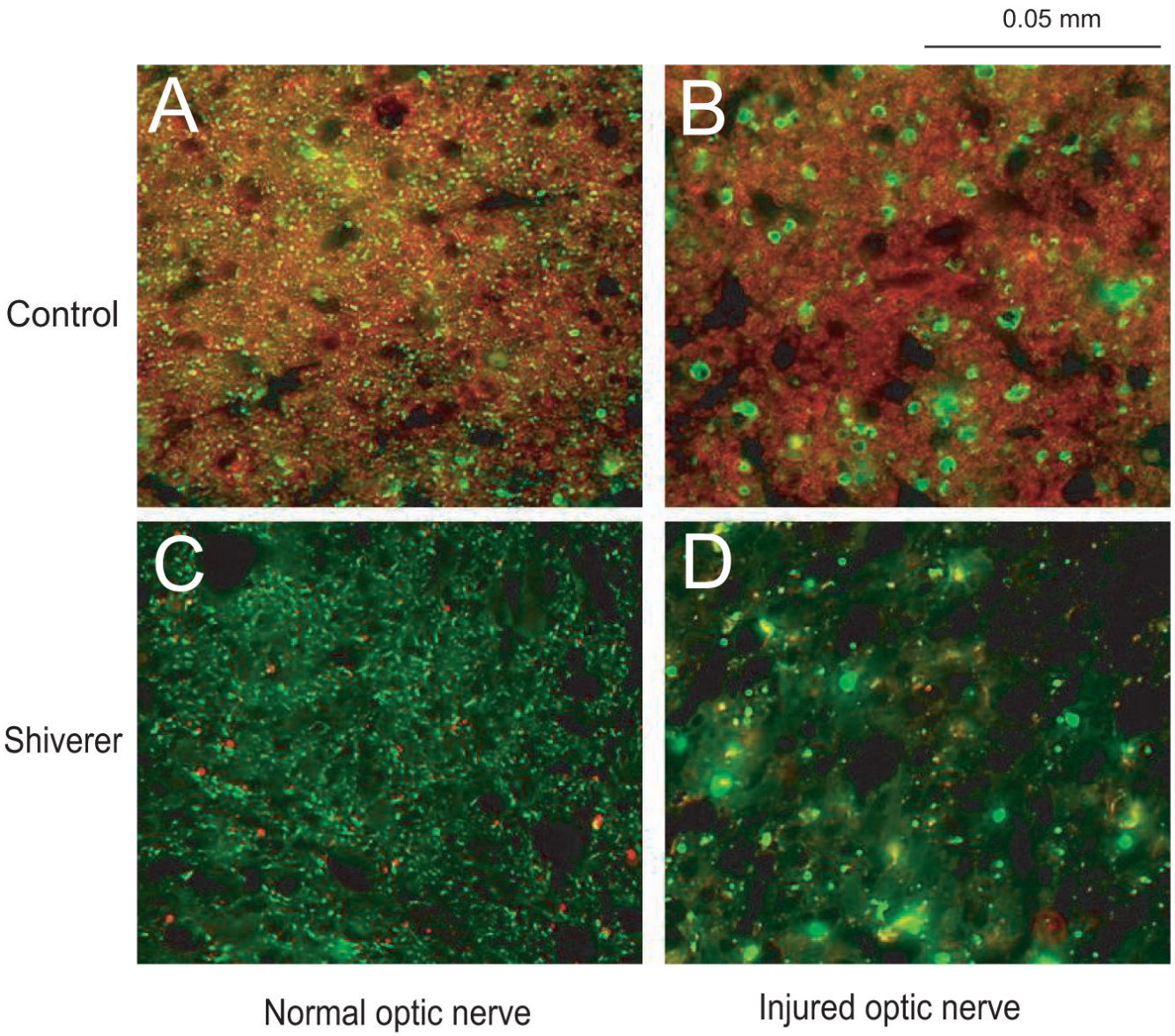

Figure 2.

Immunohistochemical results for A) uninjured optic nerve of a control mouse B) injured optic nerve of a control mouse C) uninjured optic nerve of a shiverer mouse and D) injured optic nerve of a shiverer mouse. A and B show the axonal degeneration (the green color SMI-31 labeling) and no demyelination (the red color MBP labeling) at three days after the retinal ischemia in a control mouse optic nerve; C and D show the axonal degeneration at three days after the retinal ischemia in a shiverer mouse optic nerve; both A comparing to C and B comparing to D show the dysmyelination in the shiverer mouse optic nerve.

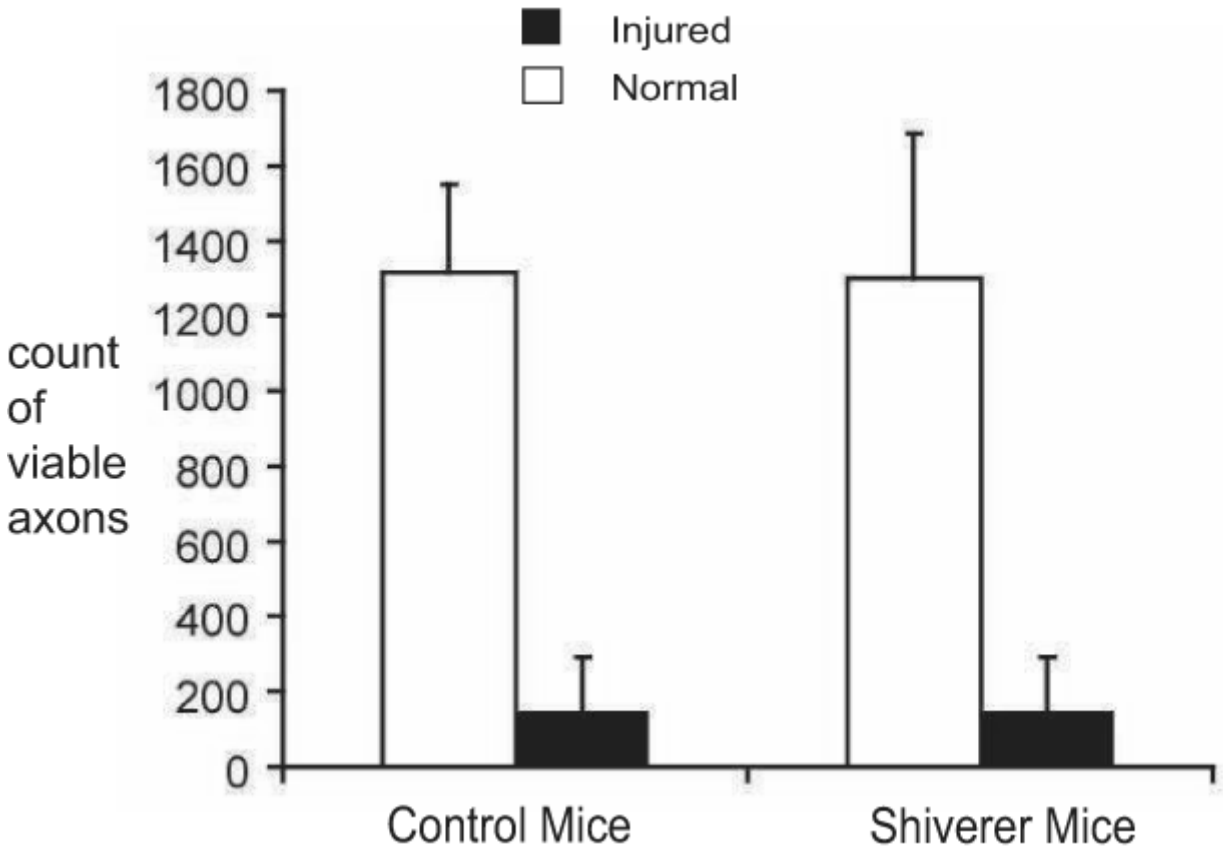

Figure 3.
Quantitative analysis of immunohistochemistry in normal (white bars) and injured (black bars) optic nerves (N = 4 for each bar). The counts of axons (pNF stained) showed that the axonal density is comparable between shieverer and control mice optic nerves. Both mice showed significant loss of normal axons in injured optic nerves at 3 days after the retinal ischemia.

Table 1

Calculated qMT and DTI parameters for mice optic nerve

Calculated qMT and DTI parameters for respective ROIs (Each pixel was fitted individually and these results were then averaged over the ROIs). We chose the whole optic nerve (excluding boundary pixels), which contains 12-20 pixels, as the ROI for each injured and uninjured optic nerve. The positioning of those ROIs were based on the relative anisotropy maps which have the most contrast between optic nerve and surrounding tissues, as shown in Figure 1. The p value (for the comparison of left injured against right uninjured) represents the statistically significant difference calculated by t-test.

			left (injured)	Right (uninjured)	p value
qMT	pool size ratio	control	0.102±0.011	0.099±0.014	0.70
		shiverer	0.069±0.004	0.076±0.007	0.07
	fast rate (s^{-1})	control	24±8	24±9	0.94
		shiverer	25±3	27±10	0.82
	slow rate (s^{-1})	control	0.92±0.09	0.92±0.08	0.90
		shiverer	0.89±0.04	0.87±0.05	0.50
DTI	radial diffusivity (μm^2 / ms)	control	0.17±0.03	0.17±0.03	0.90
		shiverer	0.22±0.02	0.22±0.04	0.84
	axial diffusivity (μm^2 / ms)	control	0.49±0.09	0.67±0.07	0.006
		shiverer	0.53±0.05	0.73±0.06	0.0002
	relative anisotropy	control	0.53±0.06	0.67±0.04	0.0011
		shiverer	0.49±0.04	0.63±0.05	0.0005